Probing Excited State Delocalization and Charge Separation in Hierarchical Perylene Diimide Materials with Time-Resolved Broadband Microscopy

Skyler R. Hollinbeck¹, Kaixuan Liu², Jean-Hubert Olivier^{2,3*}, Erik M. Grumstrup^{1,4*}

- 1) Department of Chemistry and Biochemistry, Montana State University, Bozeman MT, 59717,

 USA
 - 2) Department of Chemistry, University of Miami, Miami, FL, 33124, USA
 - 3) Department of Chemistry, University of New Mexico, Albuquerque, NM 87131, USA
- 4) Montana Materials Science Program, Montana State University, Bozeman MT, 59717, USA KEYWORDS: Ultrafast microscopy, organic crystals, heterogeneity, excited state dynamics, molecular solids, polarization dichroism, charge transfer exciton delocalization.

ABSTRACT

Using a variety of steady state and time-resolved microscopies, this work directly compares the excited state dynamics of two distinct morphologies of a hierarchical perylene diimide material: a kinetically-trapped 1D mesoscale aggregate produced with a redox-assisted self-assembly process, and a thin film produced via conventional solution-processing techniques. Although the

constituent monomer is identical for both materials, linear dichroism studies indicate that the kinetically-trapped structures possess significantly higher long-range order than the conventional thin film. A comparison of the two systems with broadband pump-probe microscopy reveals distinct differences in their excited state dynamics. In the kinetically-trapped structures, polarization-resolved kinetics, as well as a picosecond redshift of the ground state bleach provide evidence for rapid excited state delocalization, which is absent in the thin film. A comparison of transient spectra collected at 1 µs indicates the presence of long-lived charge separated states in redox treated samples, but not in the thin film. These results provide direct evidence that control of the supramolecular assembly process can be leveraged to affect the long-range order of derived PDI materials, thus enabling increased yield and lifetime of charge separated states for light harvesting applications. Furthermore, these results highlight the need for microscale broadband probes of organic materials to accurately capture the influence of local morphology on excited state functionality.

INTRODUCTION

Organic materials comprise a class of semiconductors with significant advantages, including low-cost solution-based fabrication and synthesis methods, low environmental impact, mechanical flexibility, and versatile functional tunability. The potential of tailored organic materials is well exemplified by π -conjugated molecular aggregates, where the optical and electronic properties can, in principle, be tuned not only by the *intra-molecular* structure determined by chemical design, but also by the *inter-molecular* structure and long-range ordering of the constituent monomers. Early work by Kasha serves as the foundational guide to understanding how electronic coupling between paired monomers affects absorption energy, vibronic ratios, and emission efficiencies through molecular dipole coupling. Kasha's early theoretical work has been

expanded by Spano and other,⁸⁻¹⁰ showing that in addition to the dipole coupling described by Kasha's exciton model, the optical properties of π -stacked aromatic aggregates are strongly influenced by charge-transfer superexchange interactions.^{11, 12} Strongly interacting frontier molecular orbitals and consistent long-range order are central to these intermolecular coupling mechanisms, which can give rise to a host of functionalities applicable to light harvesting applications, including delocalized charge transfer excitons with an increased propensity to charge separate.^{13, 14}

The experimental description of intermolecular coupling and how it gives rise to the optoelectronic properties in π -stacked systems, derives in large part from extensive spectroscopic comparisons of monomers to their aggregates in the solution-phase.^{6, 15-23} Perylene diimide (PDI) derivatives are an especially promising class of organic materials⁵ because of their thermal and chemical stability, high electron affinity, and strong optical absorption.²⁴ H-aggregated complexes of PDI derivatives represent a powerful testbed for probing optical and electronic tunability through modulation of interchromophore π orbital overlap, as chemical modification of side groups can be utilized to change the lowest energy stacking conformation.^{15-17, 25} The advent of such strategies to influence aggregation pathways has enabled exploration of the structure-function relationship and the emergent optoelectronic properties of supramolecular structures, as well as provided a means to design novel materials with properties targeted to specific applications.^{4, 20, 26, 27}

While spectroscopic studies of solvated aggregates are critical for establishing a fundamental understanding of intermolecular coupling, practical devices generally require condensation of the solvated precursors into a solid-state material. In the solid state, the characteristic low dielectric constant, which is in large part responsible for the superb tunability of organic materials, ^{11, 14} can

be especially disadvantageous, underpinning high exciton binding energies, strongly localized charge carriers, and sensitivity of excited state transport to vibrational coupling.²⁸ The parasitic effects of these properties are reflected in slow excited state transport, short lifetimes, and low device efficiencies.²⁴ While enhancing intermolecular orbital overlap^{11, 29} and facilitating delocalized excited states³⁰⁻³² can mitigate these deficiencies³³⁻³⁶, structural disorder introduced upon solid-state deposition begets additional difficulties in the context of both fundamental studies and in potential applications. Indeed, because the electronic coupling is highly sensitive to small perturbations in π -stacking geometry, even localized regions of structural variability can give rise to significant functional heterogeneity.^{8, 29} This localized morphological (and perhaps functional) heterogeneity is especially concerning given that the crystallization of most organic materials is driven by relatively weak non-covalent interactions. Thus, if the characterization methods employed for organic materials average over the intrinsic microscale variations in morphology, they are likely to provide an incomplete picture of the structure-function relationship.^{1,37}

In this work, we utilize broadband pump-probe microscopy with micron scale spatial resolution and femtosecond time resolution to compare the optoelectronic properties of two chemically identical PDI-derived materials with differing morphology (Fig. 1). The first sample, used as a baseline for comparison, is a thin film formed by drop-casting solvated molecular assemblies onto a substrate and allowing the solvent to slowly evaporate under near-equilibrium conditions (EQ-PDI). In the second sample, referred to as kinetically-trapped PDI (KT-PDI), the solid-state material is formed from a solution of precursor assemblies whose stacking geometry is perturbed via a redox-assisted self-assembly approach.⁴ While the modified structure of the KT-PDI assemblies has been shown to form hierarchical microscale structures and enhance exciton

coupling relative to the EQ-PDI assembly in solution, it is unclear how these traits translate to the character and dynamical evolution of the excited electronic states in solid-state materials.

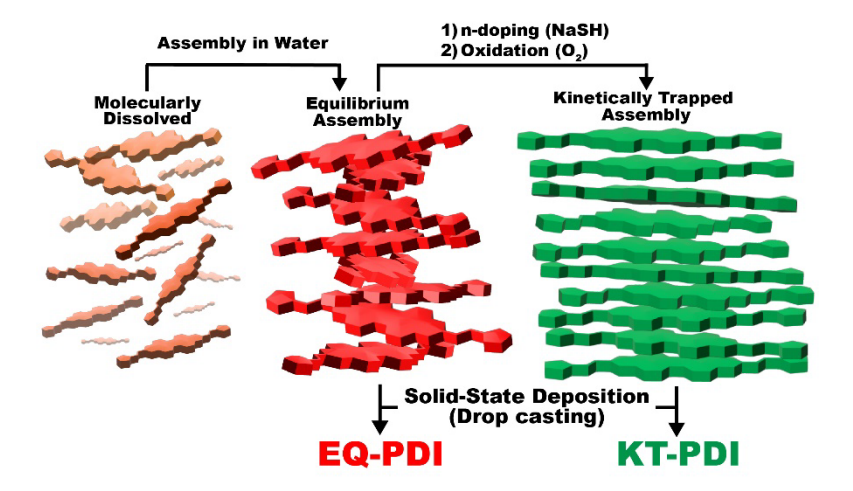


Figure 1: Depiction of the two divergent aggregation pathways of the amphiphilic PDI monomer units leading to the morphologically distinct equilibrium (EQ-PDI) and kinetically trapped (KT-PDI) solid state materials.

The direct comparison of the two materials presents a unique opportunity to study the excited state behavior of materials that feature identical molecular building blocks but evolve into morphologically distinct molecular aggregates in the solid state. In addition, this strategy allows us to determine the extent to which nanoscale assembly ordering, controlled via redox-assisted assembly in the solvated state, regulates the optoelectronic properties of solid-state hierarchical materials. We find distinct differences in both ground and excited state spectroscopies of the two materials. Relative to EQ-PDI, KT-PDI exhibits significantly enhanced linear dichroism and a distinctly red-shifted absorption spectrum, consistent with increased long-range packing order. In contrast to EQ-PDI, broadband time-resolved measurements of KT-PDI reveal a rapid redshift of the excited state spectra and anisotropy in polarization-resolved kinetics. At long times, spectroscopic signatures in KT-PDI are consistent with charge separated states persisting up to the

µs timescale. In sum, this comparative study unambiguously demonstrates that tuning intermolecular interactions of solution phase precursors can be leveraged to enhance long-range order and intermolecular coupling in the derived solid-state materials, giving rise to greater delocalization of the initially formed excited state and influencing the branching ratio of photogenerated species. These distinctions and their sources would be exceptionally difficult to disentangle using more conventional single wavelength approaches, highlighting the importance of broadband spectroscopic microscopies for the characterization of organic optoelectronic materials.

MATERIALS AND METHODS

Synthesis. Synthetic methods and characterization details of the perylene assemblies used as precursors for the solid-state samples studied here have been described in detail elsewhere.⁴ Briefly, EQ-PDI assemblies were prepared by allowing 1-(2-hydroxyethyl)-3-propyl-1H-imidizolium bromide functionalized Perylene-3,4:9,10-bisdicarboximide (PDI-C₃Im-C₂OH) monomers (Fig. 2A) to aggregate in D₂O under ambient environmental conditions. KT-PDI assemblies were produced through a reductive treatment of the D₂O suspended PDI-C₃ImC₂OH assemblies in which NaSH was incrementally added up to 2 molar equivalents (relative to initial PDI monomer concentration), followed by a single addition of NaSH solution resulting in a 5-molar equivalence of NaSH. The reduced assemblies are then oxygen-neutralized and allowed to age for 18hrs. Solid-state samples were prepared by drop casting precursor suspensions of the KT-PDI and the EQ-PDI assemblies onto fused quartz substrates. No solvent is present on the samples for any of the reported measurements.

Photophysical Measurements. Polarization-resolved brightfield microscope images are collected using an Olympus BX51 microscope equipped with a plate polarizer. Ground state

extinction spectra are collected on a custom-built microspectrometer, with the broadband light source generated by focusing 300 fs 1035 nm laser pulses into a yttrium aluminum garnet (YAG) crystal. The spot size of the continuum at the sample plane is 1.7 μ m. Note that we are unable to quantify scattering or reflection signal contributions, so extinction is defined simply as $A = 1 - \frac{T}{T_0}$. Extinction of the sample is determined by dividing the spectrum transmitted through the sample (T) by a background spectrum obtained in a region of the substrate with no sample (T₀).

Time-resolved measurements of the solid-state PDI samples were collected with a broadband pump-probe instrument previously described.³⁸ Briefly, the instrument is pumped by a 1035nm fiber laser with a 1 MHz repetition rate and a standard pulse width of 300 fs. The fundamental beam is split to form pump and probe beams, which are independently modulated with acoustooptic modulators. The pump is modulated at 31.25 kHz signal with a 50% duty cycle. The probe beam is focused into a YAG crystal to generate the supercontinuum, and the pump beam is focused into a Beta-Barium Borate crystal to produce the second harmonic 517.5 nm excitation pulse (power density limited to 58 μJ/cm²). At the fluence levels used, decay kinetics are independent of excitation density and the materials showed no sign of photodamage from the excitation or probe beams. Note also that because the probe is tightly focused, excited state diffusion out of the probe spot can contribute to the kinetic trace decay. However, calculations using standard methods show that for the measurements reported below, this effect is negligible, even under conditions of an exceptionally large excited state diffusion coefficient (Dest = 1.0 cm²/s).³⁹ A translation stage in the pump line provides the pump-probe delay and a set of galvanometer mirrors are used to spatially scan the pump relative to the probe. Spatially overlapped (pump and probe) scans of the sample are collected using a closed loop piezo stage (Mad City Labs, Nano-H100). Spatial resolution is limited by the focused beam convolution to approximately 1.7 µm. The beams are

combined with an 80/20 beam splitter before being focused onto the sample with an Olympus MPlanFL N 100X 0.9 NA objective. The transmitted light is collected with a Nikon 100x TU Plan Apo 0.9 NA objective, dispersed in a grating spectrometer, and focused onto a Teledyne Octoplus line-camera with 2048 pixels operating at 125 kHz.

RESULTS AND DISCUSSION

Morphology. Figures 2B and 2C show brightfield microscopy images of EQ-PDI thin films and KT-PDI microstructures, respectively. The EQ-PDI precursor forms thin films with variations in optical density and complex structure determined by the evaporating solvent front. Spectroscopic measurements are performed near the edge of the "coffee ring" region of the dropcast sample, which can be seen on the top right corner of Fig. 2B. The KT-PDI precursor forms long microstructures with large aspect ratios. The morphology of the KT-PDI microstructures varies between isolated long rods to crossed or bundled rods, which have been shown with transmission electron microscopy to be hierarchical superstructures of the nanoscale assemblies initially formed in solution. These mesoscale materials, which spontaneously assemble on a substrate, enable us to carefully isolate and interrogate rod-like structures like those shown in Fig. 2C to compare with the EQ-PDI film. We were unable to measure X-ray diffraction patterns from either sample while maintaining the morphologies shown in Fig. 2, however materials derived from structurally similar monomeric precursors show π - π stacking distances of 3.45 Å in drop cast films.

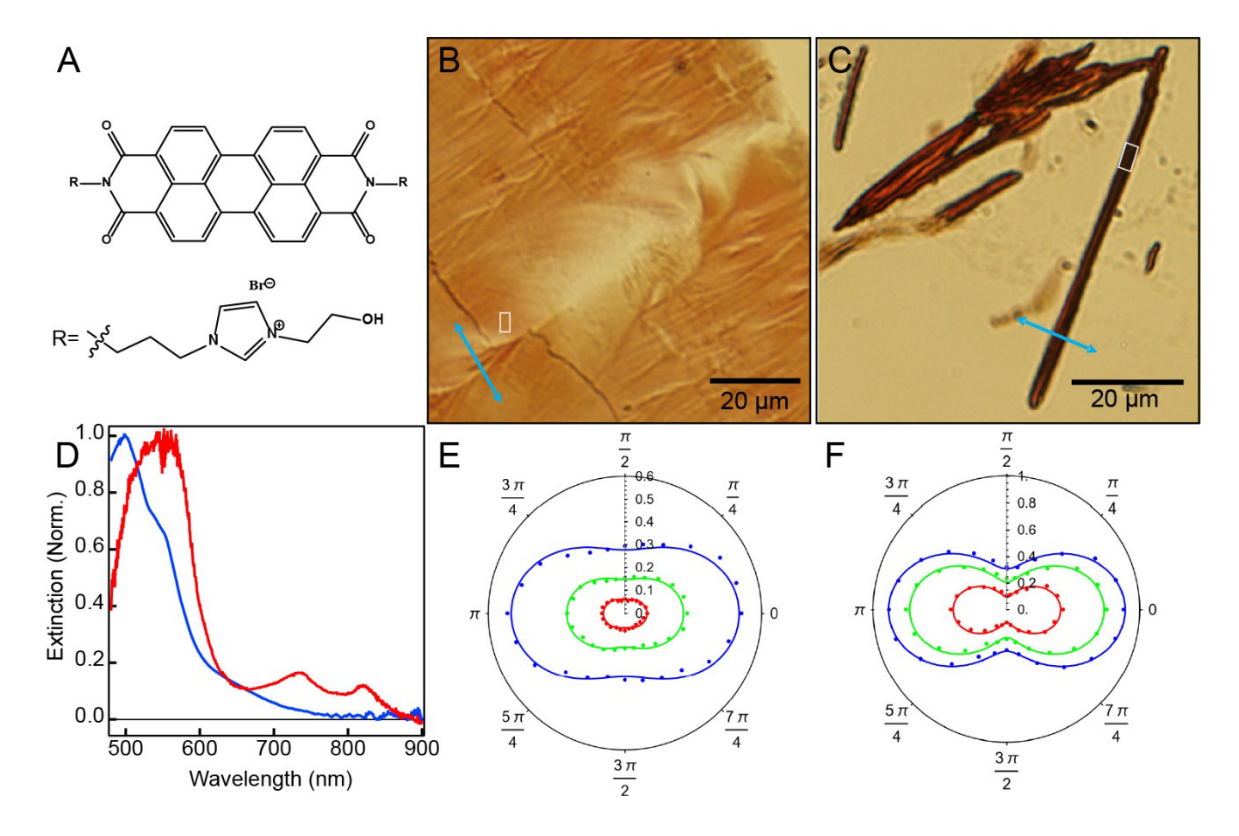


Figure 2: Steady state characterization of solid-state samples. (A) Both EQ-PDI and KT-PDI are composed of PDI-C₃Im-C₂OH monomer units. (B) Brightfield image of a dropcast film of EQ-PDI. (C) Brightfield image of the microstructures formed from KT-PDI precursors. In (B) and (C), the blue arrow indicates the polarization of the brightfield illumination. (D) Steady state extinction spectra of KT-PDI (red) and EQ-PDI (blue). Panels (E) and (F) show polarization-resolved extinction (measured in white boxes indicated in panels (B) and (C)) isolating the red, green, and blue camera channels of EQ-PDI, and KT-PDI, respectively. Solid lines are fits from Malus' law.

Ground State Extinction. Figure 2D shows a comparison of the normalized extinction spectra collected from a region \sim 1.7 μ m in diameter on each sample. The EQ-PDI spectrum shows good agreement with previously reported absorption spectra of PDI derivatives in the solid-state. ^{15, 41} The solid-state EQ-PDI spectrum is similar to that of the EQ-PDI precursor suspension (Fig. S1), although the solid-state spectrum exhibits broadened vibronic peaks and a shoulder feature near

650 nm that is absent in the suspension. The similarity of the spectra suggests that condensation has a mild effect on the electronic coupling between chromophores, with the 650 nm band perhaps indicating regions of structural disorder that lead to lower energy sites. In contrast, the KT-PDI sample shows a prominent redshifted absorption peak at 550 nm, which extends beyond 600 nm. While these lower energy transitions could be seen as evidence of low energy states arising from structural defects, linear dichroism measurements, described below, indicate that the KT-PDI sample is structurally more ordered than the EQ-PDI sample. We therefore attribute the redshifted absorption to delocalized electronic states perhaps made accessible by the altered packing geometry and stronger electron coupling in the KT-PDI microstructures. Also present in the KT-PDI spectrum are two peaks at 735 nm and 820 nm, which are also observed in solution-phase measurements (Fig. S2) of the aggregate upon electrochemical reduction. These two peaks are assigned to vibronic transitions of the electron polaron⁴² and indicate the presence of persistent reduced species from the redox-assisted self-assembly or alternatively self n-doping behavior that has been previously shown in solid-state PDI with similar imide functionalizations.^{43,44}

Polarization Dichroism. To provide insight into the microscale order of the two samples, we next turned to polarization-resolved brightfield microscopy. Examination of Fig. 2B shows large variations in the optical density with $\sim 10-20~\mu m$ long channels aligned approximately orthogonally to the edge of the film. These variations in extinction are a result of linear dichroism and show inverted contrast if the polarization of light is rotated by 90° (Fig. S3). Such polarization dichroism has been previously correlated to the long-range alignment of PDI cores, achieved, for example, through a layer-by-layer electrostatic assembly method. ^{45, 46} Given their shape and orientation relative to the film edge, we suspect the channels are local regions where alignment of the precursor assemblies was perturbed during deposition, presumably due to local differences in

the solvent evaporation rate. Qualitatively, this polarization-resolved brightfield image demonstrates the need for spatially resolved spectroscopic probes, as the local structure is clearly sensitive to microscale variations in the environment during crystallization.

Malus' law can be used to evaluate long-range chromophore ordering by quantifying extinction as a function of the angle between the polarization of the light and the electronic transition dipole moment.^{47, 48} For PDI, the largest electronic transition dipole moment is oriented along the long axis of the aromatic core of the molecule. 49 Figure 2E shows polarization-dependent extinction (1- T/T_0) collected from a 8 μ m² (2x4 μ m, drawn as a white box on Fig. 2B) region of the EQ-PDI film with homogeneous polarization response. The blue channel of the image sensor shows the strongest polarization anisotropy and is resonant with the primary excitation band in PDI.⁵⁰ For the data shown in Fig. 2E, the dichroism⁴⁶ $(D = \frac{A_{max} - A_{min}}{A_{max} + A_{min}})$, where A_{min} and A_{max} are the minimum and maximum extinction values) is found to be $D = 0.29 \, (\pm 0.01)$ for the blue channel. We note that despite using a simple drop casting procedure for the EQ-PDI film, this dichroism value is comparable to that observed in previously reported PDI films intentionally oriented with an electric field.⁴⁶ The high dichroism we observe here likely reflects a combination of the local alignment achieved by the coffee ring effect⁵¹, as well as the fact that the precursor solution is comprised of molecular assemblies rather than solvated monomers. 46 We find that for the EQ-PDI film, A_{max} is oriented parallel to the edge of the film, and A_{min} is oriented perpendicular to the film edge. However, as can be seen in Fig. 2B, there is significant microscopic heterogeneity, where nearby regions form features with differing anisotropy from each other and the spatially averaged behavior.

Whereas the EQ-PDI film has microscale regions in which the assembly orientation is altered relative to the bulk, the KT-PDI microstructures show consistent linear dichroism throughout (Fig. 2C). In Fig. 2F we show the polarization-resolved extinction from the region highlighted in Fig. 2C. In comparison to the EQ-PDI film, the KT-PDI microstructure shows even greater polarization anisotropy, with a dichroism value of 0.48 (± 0.01) on the blue channel. For KT-PDI, A_{min} is oriented parallel to the long axis of the microstructure, and A_{max} is perpendicular. Without a detailed crystal structure, it is difficult to evaluate the extent to which the dichroism value we measure in KT-PDI microstructures reflects the intrinsic packing geometry vs. conformational disorder. In the simplest case in which the plane of the PDI aromatic core is orthogonal to the long axis of the microstructure, and there are no electronic states with a transition dipole moment with a finite projection parallel to the structure's long axis, we would expect to measure a dichroism value of 1. However, more complicated stacking geometries (i.e. a slip-stack arrangement) and/or new electronic states with transition dipoles along the long axis (due perhaps to interchromophore coupling) would reduce this value from its ideal limit. Nevertheless, as a relative measure of longrange order, the greater polarization anisotropy clearly indicates that the ordering in the KT-PDI sample is significantly higher than even the locally homogeneous regions of the EQ-PDI film.

Transient microscopy. To probe how the morphological differences of the two PDI samples affect their excited state functional properties, we next turned to broadband pump-probe microscopy. The spectral resolution of broadband transient transmission measurements are useful in interpreting excited state behavior of solid organic materials where spectral resonances are 100s of nanometers broad, with strongly overlapping signals from singlet exciton absorption, ⁵² charge-transfer excimer absorption, ^{21, 22, 53} and triplet absorption. ^{23, 25, 54-56} Figure 3 summarizes the transient response of the EQ-PDI thin film up to a pump-probe delay (Δt) of 400

ps. The $\Delta t = 0$ ps pump-probe image shown in panel A is representative of the film, with spatial variation in signal intensity reflecting the microscale domains noted in the polarization-resolved brightfield images (Fig. 2B), as well as local variation in sample thickness. Although the pump polarization does not affect the shape of the transient spectra, the amplitudes of the spectral features are reduced by a factor of approximately two when the pump is polarized along the direction of minimum extinction (A_{min}). For all the pump-probe data presented here (for both EQ-PDI and KT-PDI), the pump is polarized along the direction of maximum extinction (A_{max}).

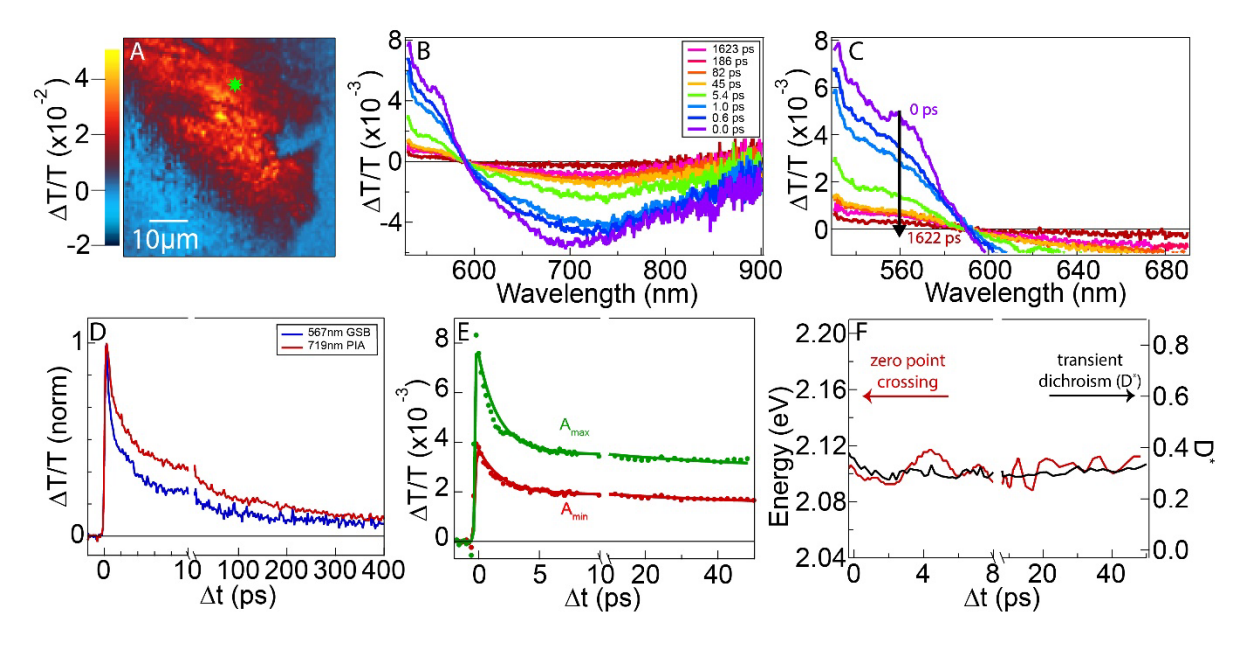


Figure 3: Excited state microscopy of EQ-PDI. (A) Spatially resolved pump-probe images of EQ-PDI (540-567nm) collected at $\Delta t = 0.1$ ps. (B) Broadband $\Delta T/T$ spectra for delay times $\Delta t = 0$, 0.6, 1.01, 5.42, 82, 186, and 1622ps) collected from the location indicated by the green star in panel A. (C) Detailed view of the ground state bleach region. (D) Comparison of normalized decay kinetics of the GSB ($\lambda = 567$ nm in blue) and the PIA ($\lambda = 719$ nm in red). (E) comparison of early time kinetics at $\lambda = 542$ nm for A_{max} and A_{min} probe polarizations. The solid traces show biexponential

fits to the data. (F) Early time zero-point crossing of the transient spectra (red) and time dependent linear dichroism (black).

Figures 3B and 3C show chirp-corrected transient transmission spectra ($\Delta T/T$), collected from the location on the EQ-PDI sample indicated by the green star in panel A. The spectra are collected with both the pump and the broadband probe polarized along A_{max} and are generally characterized by a ground state bleach (GSB) on the blue edge of the spectrum and a broad, nearly featureless photoinduced absorption (PIA) that spans 590-900 nm. The GSB closely matches the ground state absorption shown in Fig. 2D and is consistent with bleach features previously reported for other solid-state PDI films. 41 The PIA maximum undergoes a slight redshift from 706 nm to 727nm in the first few picoseconds, which we attribute to structural reorganization associated with the excited state electron configuration. The PIA and the GSB relax with similar kinetics, resulting in a nearly ideal isosbestic point at 590nm, as can be seen in the magnified view of the bleach region shown in Fig. 3C. Normalized kinetic traces of the GSB ($\lambda = 567$ nm) and PIA ($\lambda = 719$ nm) are shown in Fig. 3D, and while the kinetics at 719 nm decay slightly slower at early times due to the PIA spectral redshift, the PIA and GSB kinetics are identical after 10 ps (Fig. S4), consistent with a two level model in which the excited state population (described by the PIA) decays directly back to the ground state.

Recent solution-phase transient absorption measurements of similar PDI aggregates assign a PIA peak at $\lambda = 600$ nm to the singlet exciton and, based on spectroelectrochemical comparisons, a second PIA band with a peak at $\lambda = 720$ nm to the radical anion absorption. ^{57, 58} The broadband spectra shown in Fig. 3 show no evidence of a PIA near 600 nm immediately after photoexcitation, suggesting that the initially formed singlet excitons rapidly convert ⁵⁹ (within the instrument response time of ~300 fs) into an charge transfer excimer or charge separated state

with strong anionic character. ^{60, 61} We note that independently probing the evolution of PBI radical cation is hindered by its low extinction coefficient and strongly overlapping spectrum with both the radical anion and excitonic transient spectra. 62-64 Early time kinetics (Fig. 3E) of the bleach region ($\lambda = 542$ nm) with the probe polarized parallel (A_{max} , green) and perpendicular (A_{min}, red) to the pump show nearly identical decay kinetics, with initial lifetimes that are the same within error (A_{max}: $\tau = 1.6 ~(\pm 0.2)$ ps and A_{min}: $\tau = 1.8 ~(\pm 0.2)$ ps). In analogy to the ground state linear dichroism discussed above, we can also calculate the transient linear dichroism, defined by $D^*(\Delta t) = [(\Delta T/T)_{Amax} - (\Delta T/T)_{Amin}]/[(\Delta T/T)_{Amax} + (\Delta T/T)_{Amin}]$, which provides a measure of the linear dichroism of the excited state. As can be seen in Fig. 3F, $D^*(\Delta t)$ is delay independent and is closely comparable to the ground state dichroism (of the RGB green channel), D = 0.27. This static behavior indicates that the excited state of the EQ-PDI sample is localized with little or no evolution of the dipole along the PDI stacking axis. 65 Instead, the anisotropy observed in both the ground and excited state spectra likely reflects structural disorder (i.e. differently oriented PDI monomers) introduced during film fabrication. Together, the excited state polarization anisotropy, the well-defined isosbestic point, and the similar relaxation profiles of the GSB and PIA strongly suggest that excitation of the EQ-PDI film rapidly results in a localized charge transfer excimer that directly relaxes back to the ground state. 31, 66

Figure 4 summarizes the time-resolved microscopy results for the KT-PDI sample. The pump-probe image in Fig. 4A shows a region of the sample with two larger crossed microstructures and a small, isolated microrod. The kinetics and spectra shown in the other panels of Fig. 4 were collected on the isolated rod at the location indicated by the green star. The polarization of the

pump was adjusted to be parallel to A_{max} or perpendicular to the long axis of the crystal, and unless otherwise indicated (Fig. 4E), the probe polarization is along A_{max} for the data shown in Fig. 4.

Broadband pump-probe spectra of the KT-PDI sample, collected from $\Delta t = 0$ ps to $\Delta t = 1600$ ps, are shown in Fig. 4B and Fig. 4C. Qualitatively, the transient spectra are similar to EQ-PDI, with a GSB on the blue edge of the spectrum and broad photoinduced absorption from $\lambda \sim 600$ nm to $\lambda = 900$ nm. Closer inspection, however, reveals distinct differences between the excited state dynamics of the two samples. First, while the GSB initially looks similar to that of EQ-PDI, the bleach in KT-PDI rapidly broadens and redshifts (Fig. 4C), with a peak that moves from 570 nm to 600 nm in the first 6 ps after photoexcitation. The bleach then continues to slowly grow for ~ 200 ps before decaying on the nanosecond timescale. As a result of this spectral evolution, there is no clear isosbestic point in the transient spectra, with the zero-crossing point shifting from 590 nm at $\Delta t = 0$ ps to 660 nm at $\Delta t = 1600$ ps (Fig. 4F). The growth of the redshifted bleach feature is clearly visible in Fig. 4D, which shows a comparison between the GSB kinetics at $\lambda = 567$ nm and the PIA kinetics at $\lambda = 719$ nm. While the kinetics traces decay at comparable rates for the initial 10-20 ps, the superimposed growth and redshift of the bleach as well as overlapping PIA relaxation results in a clear rise over the next 200 ps.

A second important difference is revealed in the polarization-resolved kinetics. Whereas in EQ-PDI the early time kinetics collected at $\lambda=542$ nm measured with the two orthogonal probe polarizations were highly similar (Fig. 3E), in KT-PDI they differ substantially. For the kinetics collected with probe polarization along A_{max} (Fig. 4E, green), fits to the data recover an early decay lifetime of $\tau=0.8~(\pm0.1)$ ps, slightly shorter than the lifetimes observed in EQ-PDI for both A_{max} and A_{min} polarizations. However, as shown by the red trace in panel E, the kinetics measured along A_{min} grow in with a time constant of 265 (±15) fs and decay on much slower timescales. This

difference in polarization response leads to distinct transient dichroism behavior, as plotted in Fig. 4F. Immediately after photoexcitation, $D^*(\Delta t = 0) = 0.65$ is slightly larger than the ground state green-channel dichroism (D = 0.56), before decaying to nearly 0.0 within 10 ps. The rapid decay of $D^*(\Delta t)$ implies that, in contrast to EQ-PDI where the transient dichroism simply reflected the film morphology and was therefore time independent, in KT-PDI the excited state evolves from a state whose transition dipole projects in the same orientation as the ground state absorption to one in which the transition dipole is more strongly polarized along the π -stacking direction (long axis of the microrod).

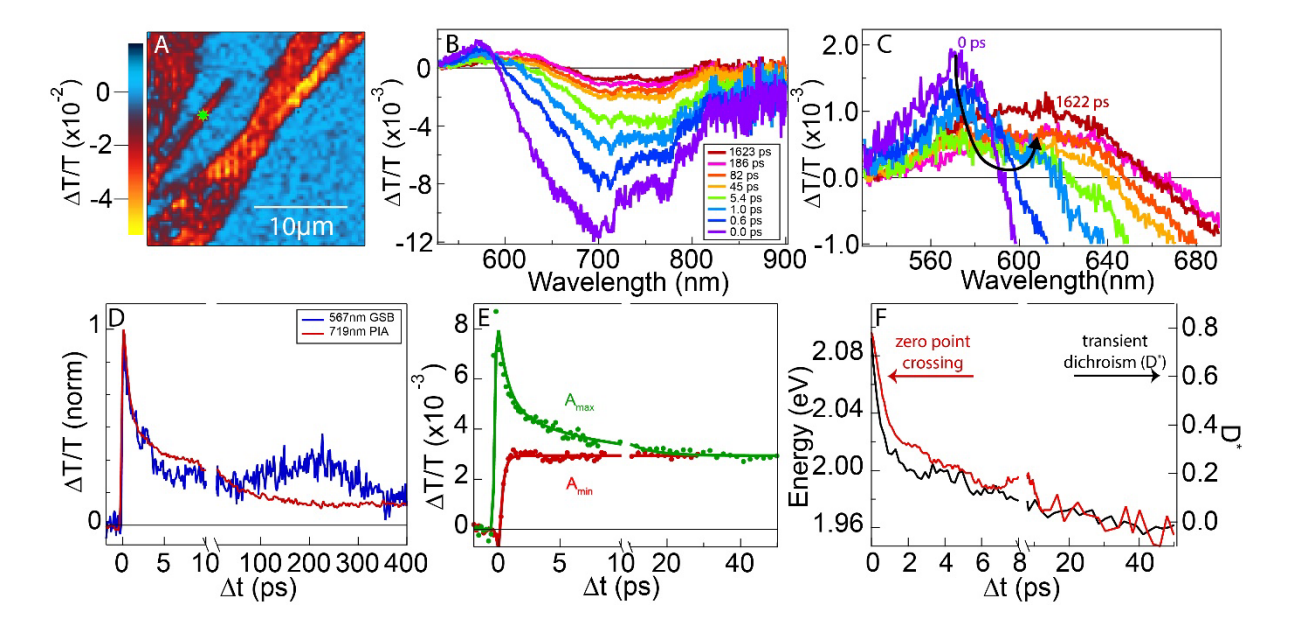


Figure 4: Excited state microscopy of EQ-PDI. (A) Spatially resolved pump-probe images of KT-PDI (670-711nm) collected at $\Delta t = 0.1$ ps. (B) Broadband $\Delta T/T$ spectra for delay times $\Delta t = 0$, 0.6, 1.01, 5.42, 82, 186, and 1622ps) collected from the location indicated by the green star in panel A, with (C) a detailed view of the ground state bleach region. (D) Comparison of normalized decay kinetics of the GSB ($\lambda = 567$ nm in blue) and the PIA ($\lambda = 719$ nm in red). (E) comparison of early time kinetics at $\lambda = 542$ nm for A_{max} and A_{min} probe polarizations. The solid traces show

biexponential fits of the data. (F) Comparison between the transient spectral zero-point crossing (red) and time dependent linear dichroism (black).

When compared with EQ-PDI, the distinct excited state spectral evolution of KT-PDI strongly suggests that its increased long-range ordering enables access to a manifold of lower energy excited states with substantial oscillator strength along the π -stacking direction. While the PIAs of both samples have anionic features which are characteristic of an excited state with charge transfer character, the redshifting GSB and the time-dependent excited state polarization dichroism show that the excited state in KT-PDI is not immediately trapped like in EQ-PDI, but evolves for 10s – 100s of ps. A comparative plot of the spectral redshift of the GSB and the transient linear dichroism (Fig. 4F) shows that the time evolution of the two spectroscopic signatures is nearly identical, indicating that the two processes are reporting on the same excited state relaxation process. Together, these spectroscopic observables suggest that after photoexcitation of KT-PDI, the initially photogenerated state relaxes on the picosecond timescale to form a delocalized chargetransfer exciton. 41, 59 Although the susceptibility to photodamage and the broad spectral resonances of these solid state materials make it difficult to estimate a delocalization length⁶⁷⁻⁶⁹, similar delocalization behavior has been observed in analogous non-covalent organic solids, where increased molecular ordering has been correlated with delocalization of charge-transfer excitons over multiple molecular pairs.^{29, 70} It is especially noteworthy that because the two films are assembled from the same monomer subunit, this distinct difference in photophysical behavior can only be a result of the different assembly conditions and morphologies of the two samples.

Delocalized charge transfer excitons are known to help facilitate higher rates of charge separation^{14, 29, 36} and lead to better efficiencies in light-harvesting devices.⁷¹ To test whether the enhanced delocalization observed on the ps-ns timescale in KT-PDI resulted in any difference in

excited state evolution and charge carrier formation, we next measured transient spectra from both samples at a delay time of $\Delta t = 1~\mu s$. To achieve this long pump-probe delay we adjusted the acousto-optic modulator timing values to select pump and probe pulses with a 1 μ s separation. Figure 5A shows a comparison of these long-lived spectral signatures for both EQ-PDI (blue) and KT-PDI (black). For EQ-PDI (blue) the transient spectra are characterized by a low amplitude signal (~one hundredth of $\Delta t = 0~ps$ signal) that closely resembles the early time transient transmission spectra (Fig. 3). This similarity of the early and late time spectra suggests that a small subpopulation of long-lived excimers persist even to μ s timescales. Given the spectral similarity of the early and late time populations, it is difficult to precisely explain the origin of this long-lived portion of the population. However, it may be that microscopic structural heterogeneities facilitate the formation of the long-lived states that are decoupled from the dominant relaxation pathways.

In contrast to EQ-PDI, the 1 μ s KT-PDI transient spectra has significant amplitude (~one tenth of $\Delta t = 0$ ps signal) and is distinct from the early time transient transmission spectra, with sharp positive peaks at 818 nm and at 726 nm overlaying a broad PIA. The distinctive peaks closely align with the monoanionic vibronic absorption features observed in ground state extinction spectra of KT-PDI.^{4, 43, 44, 72} Comparison of the transient spectra with the ground state extinction spectra shows the transient features do not arise from a simple bleaching of the ground state spectrum. Whereas the band near 720 nm is stronger than that near 820 nm in the ground state extinction spectrum (Fig. 2D), the relative intensities are reversed in the transient spectrum, with the band at 818 nm nearly a factor of three more intense than that at 726 nm. Instead, we assign the long-lived transient spectrum to an electron polaron, resulting from charge separation of the delocalized charge-transfer exciton. Comparison of the 1 μ s KT-PDI transient transmission spectrum to a calculated difference spectrum obtained from chemical reduction supports this

assignment (Fig. 5b). Shown in red in Fig. 5b is the differential spectrum determined by subtracting the solution-phase transmission spectrum of KT-PDI assemblies at 0.3 equivalents sacrificial electron donor (NaSH) concentration from that obtained at 0.5 equivalents. The difference spectrum shows that as the electron concentration in the assemblies increases, the features associated with monoanion absorption bleach and transmission near 650 nm decreases. Although not a perfect match, the simulated spectral evolution is consistent with the spectral features observed in pump-probe data. Differences between the two spectra likely arise from radical cation contributions, including ground state bleaching (particularly around 600 nm) and the broad PIA evident in the $\Delta t \sim 1$ ns transient spectra (Fig. 4D). While further study is necessary, we also note that aromatic dianion stabilization or the formation of negative trions may help stabilize these long-lived states with anionic spectral signatures.^{44, 73}

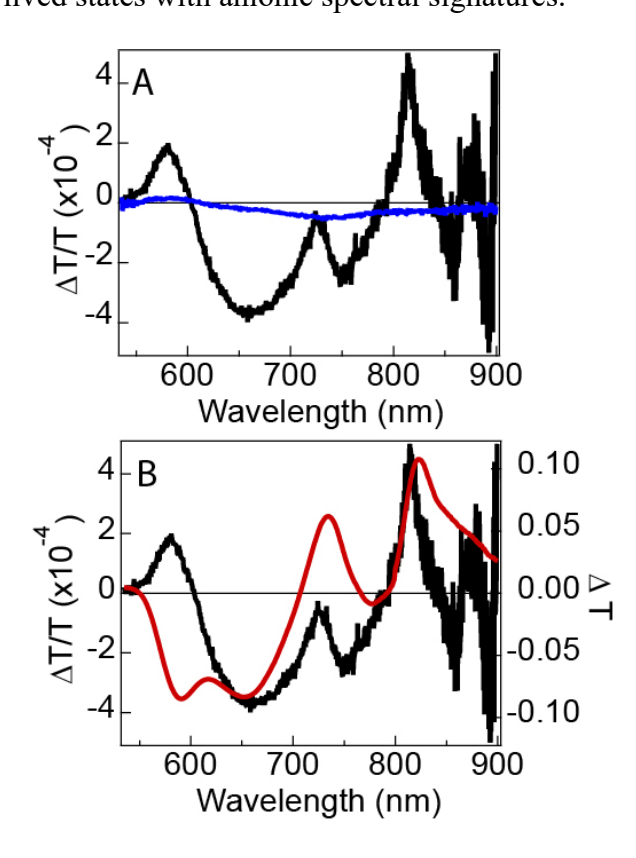


Figure 5: Long lived transient transmission signal $\Delta t = 1$ µs after photoexcitation (Panel A). The blue trace corresponds to EQ-PDI (A_{max}) and black to KT-PDI (A_{max}). Panel B compares the long-lived KT-PDI spectra (black) to the differential spectrum (red) calculated from steady state spectra collected for different levels of PDI-C₃Im-C₂OH chemical reduction ($T_{0.5eq,NaSH} - T_{0.3eq,NaSH}$).

The spectroscopic evidence of long-lived electron polarons in KT-PDI and its absence in EQ-PDI can be understood by considering the differences in early time excited state evolution for the two samples. For EQ-PDI, we observe no evidence of excited state delocalization (Fig. 3) in the early time dynamics. It appears that in EQ-PDI, the reduced crystalline order (Fig. 2E) results in localized excited states, which directly relax to the ground state. In contrast, for KT-PDI we observe spectral redshifting and evolution of the polarization dichroism (Fig. 4), both of which indicate that initially photogenerated states undergo rapid relaxation to form delocalized charge-transfer states. Because delocalization will reduce the Coulomb coupling between charges, these states are more likely to charge separate to form polarons. 12, 29, 71, 74 Delocalization will also reduce phonon coupling, which may make the nascent polarons more mobile. Thus, the formation and perhaps greater mobility of delocalized polarons leads to a long-lived population that persists on timescales greater than 1 μs.

CONCLUSION

This work highlights the importance of non-covalent assembly processes in determining the solid-state morphology of derived molecular aggregate materials. Using both steady state and time-resolved microscopies, fundamental differences in the nature and evolution of excited state species are identified in morphologically distinct PDI-C₃ImC₂OH aggregates. Brightfield microscopy and linear dichroism indicate that relative to EQ-PDI, the long-range ordering of KT-PDI is significantly enhanced. Broadband transient spectra, collected using a pump-probe microscope to

ensure that the probed regions of both samples are structurally homogeneous, are consistent with formation of an initial excited state population with significant charge transfer character. However, in KT-PDI, increased electronic coupling and greater long-range order result in excited state evolution on the 1s - 100s of ps timescale to a delocalized charge-transfer state poised for charge separation. At long times ($\Delta t = 1 \mu s$), only KT-PDI exhibits transient spectral features that are characteristic of electron polaron formation, highlighting the importance of delocalization in charge-separated excited state formation. These results confirm the potential of controlling solution-phase aggregation pathways to affect the nature and trajectory of photoexcited species in solid-state organic materials derived from molecular aggregate precursors. These approaches may provide a reliable approach for the formation of solid state materials that facilitate charge separation, with substantive implications for both photovoltaic and photocatalytic applications. ¹⁴, 35, 71 Finally, we note that the combination of structural heterogeneity and broad spectral resonances that are characteristic of solid-state molecular solids pose a significant barrier to photophysical understanding of these challenging systems. Ensemble spectroscopies necessarily integrate over structural variation, and single wavelength microscopies can miss important spectral dynamics. In this respect, broadband time-resolved microscopy offers enormous potential as a tool to elucidate the particularly sensitive structure-function relationship in molecular solids.

ASSOCIATED CONTENT

Supporting Information. Comparison of ground state extinction spectra for precursor solutions and solid-state samples, polarization-resolved brightfield images of EQ-PDI film, Additional time-resolved kinetics comparisons

AUTHOR INFORMATION

Corresponding Author

*erik.grumstrup@montana.edu

*iholivier67@unm.edu

Acknowledgements

SRH and EMG supported by NSF award CHE-2154448. EMG and JHO acknowledge support of the Arnold and Mabel Beckman Foundation.

REFERENCES

- (1) Fahlman, M.; Fabiano, S.; Gueskine, V.; Simon, D.; Berggren, M.; Crispin, X., Interfaces in organic electronics. *Nature Reviews Materials* **2019**, *4*, 627-650. https://doi.org/10.1038/s41578-019-0127-y
- (2) Zhang, Q.; Hu, W.; Sirringhaus, H.; Müllen, K., Recent Progress in Emerging Organic Semiconductors. *Advanced Materials* **2022**, *34*, 2108701. https://doi.org/https://doi.org/10.1002/adma.202108701
- (3) Yang, S.-Y.; Qu, Y.-K.; Liao, L.-S.; Jiang, Z.-Q.; Lee, S.-T., Research Progress of Intramolecular π -Stacked Small Molecules for Device Applications. *Advanced Materials* **2022**, *34*, 2104125. https://doi.org/https://doi.org/10.1002/adma.202104125
- (4) Liu, K.; Mukhopadhyay, A.; Ashcraft, A.; Liu, C.; Levy, A.; Blackwelder, P.; Olivier, J.-H., Reconfiguration of π-conjugated superstructures enabled by redox-assisted assembly. *Chemical Communications* **2019**, *55*, 5603-5606. https://doi.org/10.1039/C9CC01939A
- (5) Li, Y.; Zhang, X.; Liu, D., Recent developments of perylene diimide (PDI) supramolecular photocatalysts: A review. *Journal of Photochemistry and Photobiology C: Photochemistry Reviews* **2021**, *48*, 100436. https://doi.org/https://doi.org/10.1016/j.jphotochemrev.2021.100436
- (6) Zhang, F.; Ma, Y.; Chi, Y.; Yu, H.; Li, Y.; Jiang, T.; Wei, X.; Shi, J., Self-assembly, optical and electrical properties of perylene diimide dyes bearing unsymmetrical substituents at bay position. *Scientific Reports* **2018**, *8*, 8208. https://doi.org/10.1038/s41598-018-26502-5
- (7) Kasha, M.; Rawls, H. R.; El-Bayoumi, M. A., The exciton model in molecular spectroscopy. *Pure and Applied Chemistry* **1965**, *11*, 371-392. https://doi.org/doi:10.1351/pac196511030371
- (8) Henson, Z. B.; Müllen, K.; Bazan, G. C., Design strategies for organic semiconductors beyond the molecular formula. *Nature Chemistry* **2012**, *4*, 699-704. https://doi.org/10.1038/nchem.1422
- (9) Sutton, C.; Risko, C.; Brédas, J.-L., Noncovalent Intermolecular Interactions in Organic Electronic Materials: Implications for the Molecular Packing vs Electronic Properties of Acenes. *Chemistry of Materials* **2016**, *28*, 3-16. https://doi.org/10.1021/acs.chemmater.5b03266

- (10) Vura-Weis, J.; Ratner, M. A.; Wasielewski, M. R., Geometry and Electronic Coupling in Perylenediimide Stacks: Mapping Structure—Charge Transport Relationships. *Journal of the American Chemical Society* **2010**, *132*, 1738-1739. https://doi.org/10.1021/ja907761e
- (11) Hestand, N. J.; Spano, F. C., Molecular Aggregate Photophysics beyond the Kasha Model: Novel Design Principles for Organic Materials. *Accounts of Chemical Research* **2017**, 50, 341-350. https://doi.org/10.1021/acs.accounts.6b00576
- (12) Hestand, N. J.; Spano, F. C., Expanded Theory of H- and J-Molecular Aggregates: The Effects of Vibronic Coupling and Intermolecular Charge Transfer. *Chemical Reviews* **2018**, *118*, 7069-7163. https://doi.org/10.1021/acs.chemrev.7b00581
- (13) Liu, K.; Paulino, V.; Mukhopadhyay, A.; Bernard, B.; Kumbhar, A.; Liu, C.; Olivier, J.-H., How to reprogram the excitonic properties and solid-state morphologies of π -conjugated supramolecular polymers. *Phys. Chem. Chem. Phys.* **2021**, *23*, 2703-2714. https://doi.org/10.1039/D0CP04819D
- (14) Bernardo, B.; Cheyns, D.; Verreet, B.; Schaller, R. D.; Rand, B. P.; Giebink, N. C., Delocalization and dielectric screening of charge transfer states in organic photovoltaic cells. *Nature Communications* **2014**, *5*, 3245. https://doi.org/10.1038/ncomms4245
- (15) Balakrishnan, K.; Datar, A.; Naddo, T.; Huang, J.; Oitker, R.; Yen, M.; Zhao, J.; Zang, L., Effect of Side-Chain Substituents on Self-Assembly of Perylene Diimide Molecules: Morphology Control. *Journal of the American Chemical Society* **2006**, *128*, 7390-7398. https://doi.org/10.1021/ja061810z
- (16) Dirian, K.; Bauroth, S.; Roth, A.; Syrgiannis, Z.; Rigodanza, F.; Burian, M.; Amenitsch, H.; Sharapa, D. I.; Prato, M.; Clark, T., *et al.*, A water-soluble, bay-functionalized perylenediimide derivative correlating aggregation and excited state dynamics. *Nanoscale* **2018**, *10*, 2317-2326. https://doi.org/10.1039/C7NR07870F
- (17) Görl, D.; Zhang, X.; Würthner, F., Molecular Assemblies of Perylene Bisimide Dyes in Water. *Angewandte Chemie International Edition* **2012**, *51*, 6328-6348. https://doi.org/https://doi.org/10.1002/anie.201108690
- (18) Korevaar, P. A.; de Greef, T. F. A.; Meijer, E. W., Pathway Complexity in π -Conjugated Materials. *Chemistry of Materials* **2014**, *26*, 576-586. https://doi.org/10.1021/cm4021172
- (19) Zhong, C. J.; Kwan, W. S. V.; Miller, L. L., Self-assembly of delocalized .pi.-stacks in solution. Assessment of structural effects. *Chemistry of Materials* **1992**, *4*, 1423-1428. https://doi.org/10.1021/cm00024a052
- (20) Feng, J.; Jiang, W.; Wang, Z., Synthesis and Application of Rylene Imide Dyes as Organic Semiconducting Materials. *Chemistry An Asian Journal* **2018**, *13*, 20-30. https://doi.org/https://doi.org/10.1002/asia.201701424
- (21) Brown, K. E.; Salamant, W. A.; Shoer, L. E.; Young, R. M.; Wasielewski, M. R., Direct Observation of Ultrafast Excimer Formation in Covalent Perylenediimide Dimers Using Near-Infrared Transient Absorption Spectroscopy. *The Journal of Physical Chemistry Letters* **2014**, *5*, 2588-2593. https://doi.org/10.1021/jz5011797
- (22) Cook, R. E.; Phelan, B. T.; Kamire, R. J.; Majewski, M. B.; Young, R. M.; Wasielewski, M. R., Excimer Formation and Symmetry-Breaking Charge Transfer in Cofacial Perylene Dimers. *The Journal of Physical Chemistry A* **2017**, *121*, 1607-1615. https://doi.org/10.1021/acs.jpca.6b12644

- (23) Ford, W. E.; Kamat, P. V., Photochemistry of 3,4,9,10-perylenetetracarboxylic dianhydride dyes. 3. Singlet and triplet excited-state properties of the bis(2,5-di-tert-butylphenyl)imide derivative. *The Journal of Physical Chemistry* **1987**, *91*, 6373-6380. https://doi.org/10.1021/j100309a012
- (24) Cheng, P.; Zhao, X.; Zhan, X., Perylene Diimide-Based Oligomers and Polymers for Organic Optoelectronics. *Accounts of Materials Research* **2022**, *3*, 309-318. https://doi.org/10.1021/accountsmr.1c00191
- (25) Eaton, S. W.; Shoer, L. E.; Karlen, S. D.; Dyar, S. M.; Margulies, E. A.; Veldkamp, B. S.; Ramanan, C.; Hartzler, D. A.; Savikhin, S.; Marks, T. J., *et al.*, Singlet Exciton Fission in Polycrystalline Thin Films of a Slip-Stacked Perylenediimide. *Journal of the American Chemical Society* **2013**, *135*, 14701-14712. https://doi.org/10.1021/ja4053174
- (26) Hu, Z.; Haws, R. T.; Fei, Z.; Boufflet, P.; Heeney, M.; Rossky, P. J.; Vanden Bout, D. A., Impact of backbone fluorination on nanoscale morphology and excitonic coupling in polythiophenes. *Proceedings of the National Academy of Sciences* **2017**, *114*, 5113-5118. https://doi.org/doi.10.1073/pnas.1620722114
- (27) Würthner, F., Perylene bisimide dyes as versatile building blocks for functional supramolecular architectures. *Chemical Communications* **2004**, 1564-1579. https://doi.org/10.1039/B401630K
- (28) Hoffmann, M., Mixing of Frenkel and Charge-Transfer Excitons and Their Quantum Confinement in Thin Films. In *Thin Films and Nanostructures*, Academic Press: 2003; Vol. 31, pp 221-292.
- (29) Chen, X.-K.; Ravva, M. K.; Li, H.; Ryno, S. M.; Brédas, J.-L., Effect of Molecular Packing and Charge Delocalization on the Nonradiative Recombination of Charge-Transfer States in Organic Solar Cells. *Advanced Energy Materials* **2016**, *6*, 1601325. https://doi.org/https://doi.org/10.1002/aenm.201601325
- (30) Chang, J.-F.; Sakanoue, T.; Olivier, Y.; Uemura, T.; Dufourg-Madec, M.-B.; Yeates, S. G.; Cornil, J.; Takeya, J.; Troisi, A.; Sirringhaus, H., Hall-Effect Measurements Probing the Degree of Charge-Carrier Delocalization in Solution-Processed Crystalline Molecular Semiconductors. *Physical Review Letters* **2011**, *107*, 066601. https://doi.org/10.1103/PhysRevLett.107.066601
- (31) Kaufmann, C.; Kim, W.; Nowak-Król, A.; Hong, Y.; Kim, D.; Würthner, F., Ultrafast Exciton Delocalization, Localization, and Excimer Formation Dynamics in a Highly Defined Perylene Bisimide Quadruple π-Stack. *Journal of the American Chemical Society* **2018**, *140*, 4253-4258. https://doi.org/10.1021/jacs.7b11571
- (32) Spano, F. C., The Spectral Signatures of Frenkel Polarons in H- and J-Aggregates. *Accounts of Chemical Research* **2010**, *43*, 429-439. https://doi.org/10.1021/ar900233v
- (33) Stehr, V.; Fink, R. F.; Engels, B.; Pflaum, J.; Deibel, C., Singlet Exciton Diffusion in Organic Crystals Based on Marcus Transfer Rates. *Journal of Chemical Theory and Computation* **2014**, *10*, 1242-1255. https://doi.org/10.1021/ct500014h
- (34) Marcus, R. A., Electron transfer reactions in chemistry. Theory and experiment. *Reviews of Modern Physics* **1993**, *65*, 599-610. https://doi.org/10.1103/RevModPhys.65.599
- (35) Bakulin, A. A.; Rao, A.; Pavelyev, V. G.; van Loosdrecht, P. H. M.; Pshenichnikov, M. S.; Niedzialek, D.; Cornil, J.; Beljonne, D.; Friend, R. H., The Role of Driving Energy and Delocalized States for Charge Separation in Organic Semiconductors. *Science* **2012**, *335*, 1340-1344. https://doi.org/doi:10.1126/science.1217745

- (36) Gélinas, S.; Rao, A.; Kumar, A.; Smith, S. L.; Chin, A. W.; Clark, J.; van der Poll, T. S.; Bazan, G. C.; Friend, R. H., Ultrafast Long-Range Charge Separation in Organic Semiconductor Photovoltaic Diodes. *Science* **2014**, *343*, 512-516. https://doi.org/doi:10.1126/science.1246249
- (37) Beaujuge, P. M.; Fréchet, J. M. J., Molecular Design and Ordering Effects in π -Functional Materials for Transistor and Solar Cell Applications. *Journal of the American Chemical Society* **2011**, *133*, 20009-20029. https://doi.org/10.1021/ja2073643
- (38) Piland, G.; Grumstrup, E. M., High-Repetition Rate Broadband Pump—Probe Microscopy. *The Journal of Physical Chemistry A* **2019**, *123*, 8709-8716. https://doi.org/10.1021/acs.jpca.9b03858
- (39) Grumstrup, E. M.; Gabriel, M. M.; Pinion, C. W.; Parker, J. K.; Cahoon, J. F.; Papanikolas, J. M., Reversible Strain-Induced Electron–Hole Recombination in Silicon Nanowires Observed with Femtosecond Pump–Probe Microscopy. *Nano Letters* **2014**, *14*, 6287-6292. https://doi.org/10.1021/nl5026166
- (40) King, A. J.; Paulino, V. A.; Hollinbeck, S. R.; Tsironi, I.; Maleszka, J. A.; Olivier, J.-H.; Grumstrup, E. M., Covalently Tethered Assemblies Improve Energetic Homogeneity and Exciton Transport in Organic Materials. *ACS Materials Letters* **2024**, *6*, 1404-1410. https://doi.org/10.1021/acsmaterialslett.4c00279
- (41) Pandya, R.; Chen, R. Y. S.; Gu, Q.; Gorman, J.; Auras, F.; Sung, J.; Friend, R.; Kukura, P.; Schnedermann, C.; Rao, A., Femtosecond Transient Absorption Microscopy of Singlet Exciton Motion in Side-Chain Engineered Perylene-Diimide Thin Films. *The Journal of Physical Chemistry A* **2020**, *124*, 2721-2730. https://doi.org/10.1021/acs.jpca.0c00346
- (42) Gosztola, D.; Niemczyk, M. P.; Svec, W.; Lukas, A. S.; Wasielewski, M. R., Excited Doublet States of Electrochemically Generated Aromatic Imide and Diimide Radical Anions. *The Journal of Physical Chemistry A* **2000**, *104*, 6545-6551. https://doi.org/10.1021/jp000706f
- (43) Powell, D.; Zhang, X.; Nwachukwu, C. I.; Miller, E. J.; Hansen, K. R.; Flannery, L.; Ogle, J.; Berzansky, A.; Labram, J. G.; Roberts, A. G., *et al.*, Establishing Self-Dopant Design Principles from Structure–Function Relationships in Self-n-Doped Perylene Diimide Organic Semiconductors. *Advanced Materials* **2022**, 2204656. https://doi.org/https://doi.org/10.1002/adma.202204656
- (44) Powell, D.; Rhodes, Z.; Zhang, X.; Miller, E. J.; Jonely, M.; Hansen, K. R.; Nwachukwu, C. I.; Roberts, A. G.; Wang, H.; Noriega, R., *et al.*, Photoactivation Properties of Self-n-Doped Perylene Diimides: Concentration-dependent Radical Anion and Dianion Formation. *ACS Materials Au* **2022**, *2*, 482-488. https://doi.org/10.1021/acsmaterialsau.2c00019
- (45) Weitzel, C. R., Investigation into water-soluble perylene diimides for thin film formation. *Kansas State University* **2008**. https://doi.org/http://hdl.handle.net/2097/778
- (46) Weitzel, C. R.; Everett, T. A.; Higgins, D. A., Aggregation and Its Influence on Macroscopic In-Plane Organization in Thin Films of Electrostatically Self-Assembled Perylene-Diimide/Polyelectrolyte Nanofibers. *Langmuir* **2009**, *25*, 1188-1195. https://doi.org/10.1021/la803177n
- (47) Gregoriou, V. G.; Tzavalas, S.; Bollas, S. T., Angular Dependence in Infrared Linear Dichroism: A Reevaluation of the Theory. *Applied Spectroscopy* **2004**, *58*, 655-661. https://doi.org/10.1366/000370204873024

- (48) Mayerhöfer, T. G., Employing Theories Far beyond Their Limits Linear Dichroism Theory. *ChemPhysChem* **2018**, *19*, 2123-2130. https://doi.org/https://doi.org/10.1002/cphc.201800214
- (49) Kistler, K. A.; Pochas, C. M.; Yamagata, H.; Matsika, S.; Spano, F. C., Absorption, Circular Dichroism, and Photoluminescence in Perylene Diimide Bichromophores: Polarization-Dependent H- and J-Aggregate Behavior. *The Journal of Physical Chemistry B* **2012**, *116*, 77-86. https://doi.org/10.1021/jp208794t
- (50) Zou, X.; Zhang, Y.; Lin, R.; Gong, G.; Wang, S.; Zhu, S.; Wang, Z., Pixel-level Bayer-type colour router based on metasurfaces. *Nature Communications* **2022**, *13*, 3288. https://doi.org/10.1038/s41467-022-31019-7
- (51) Mampallil, D.; Eral, H. B., A review on suppression and utilization of the coffeering effect. *Advances in Colloid and Interface Science* **2018**, *252*, 38-54. https://doi.org/10.1016/j.cis.2017.12.008
- (52) Giaimo, J. M.; Lockard, J. V.; Sinks, L. E.; Scott, A. M.; Wilson, T. M.; Wasielewski, M. R., Excited Singlet States of Covalently Bound, Cofacial Dimers and Trimers of Perylene-3,4:9,10-bis(dicarboximide)s. *The Journal of Physical Chemistry A* **2008**, *112*, 2322-2330. https://doi.org/10.1021/jp710847q
- (53) Son, M.; Park, K. H.; Shao, C.; Würthner, F.; Kim, D., Spectroscopic Demonstration of Exciton Dynamics and Excimer Formation in a Sterically Controlled Perylene Bisimide Dimer Aggregate. *The Journal of Physical Chemistry Letters* **2014**, *5*, 3601-3607. https://doi.org/10.1021/jz501953a
- (54) Le, A. K.; Bender, J. A.; Arias, D. H.; Cotton, D. E.; Johnson, J. C.; Roberts, S. T., Singlet Fission Involves an Interplay between Energetic Driving Force and Electronic Coupling in Perylenediimide Films. *Journal of the American Chemical Society* **2018**, *140*, 814-826. https://doi.org/10.1021/jacs.7b11888
- (55) Aulin, Y. V.; Felter, K. M.; Günbas, D. D.; Dubey, R. K.; Jager, W. F.; Grozema, F. C., Morphology-Independent Efficient Singlet Exciton Fission in Perylene Diimide Thin Films. *ChemPlusChem* **2018**, *83*, 230-238. https://doi.org/10.1002/cplu.201700449
- (56) Felter, K. Triplet Dynamics in Crystalline Perylene Diimides. PhD thesis, Delft University of Technology, 2020. https://doi.org/10.4233/uuid:5137711f-d5e6-41b6-ac7a-34c6c5e29caf
- (57) Paulino, V.; Cadena, D. M.; Liu, K.; Mukhopadhyay, A.; Roberts, S. T.; Olivier, J.-H., The Length of Molecular Tethers Can Be Used to Control the Structure and Electronic Properties of Stapled Supramolecular Polymers. *Chemistry of Materials* **2022**, *34*, 6518-6528. https://doi.org/10.1021/acs.chemmater.2c01353
- (58) Lin, C.; Kim, T.; Schultz, J. D.; Young, R. M.; Wasielewski, M. R., Accelerating symmetry-breaking charge separation in a perylenediimide trimer through a vibronically coherent dimer intermediate. *Nature Chemistry* **2022**, 786-793. https://doi.org/10.1038/s41557-022-00927-y
- (59) Lim, J. M.; Kim, P.; Yoon, M.-C.; Sung, J.; Dehm, V.; Chen, Z.; Würthner, F.; Kim, D., Exciton delocalization and dynamics in helical π -stacks of self-assembled perylene bisimides. *Chemical Science* **2013**, *4*, 388-397. https://doi.org/10.1039/C2SC21178E
- (60) Katoh, R.; Sinha, S.; Murata, S.; Tachiya, M., Origin of the stabilization energy of perylene excimer as studied by fluorescence and near-IR transient absorption spectroscopy. *Journal of Photochemistry and Photobiology A: Chemistry* **2001**, *145*, 23-34. https://doi.org/https://doi.org/10.1016/S1010-6030(01)00562-7

- (61) Myong, M. S.; Zhou, J.; Young, R. M.; Wasielewski, M. R., Charge-Transfer Character in Excimers of Perylenediimides Self-Assembled on Anodic Aluminum Oxide Membrane Walls. *The Journal of Physical Chemistry C* **2020**, *124*, 4369-4377. https://doi.org/10.1021/acs.jpcc.9b10805
- (62) Kim, W.; Nowak-Król, A.; Hong, Y.; Schlosser, F.; Würthner, F.; Kim, D., Solvent-Modulated Charge-Transfer Resonance Enhancement in the Excimer State of a Bay-Substituted Perylene Bisimide Cyclophane. *J Phys Chem Lett* **2019**, *10*, 1919-1927. https://doi.org/10.1021/acs.jpclett.9b00357
- (63) Würthner, F.; Sautter, A.; Schmid, D.; Weber, P. J. A., Fluorescent and Electroactive Cyclic Assemblies from Perylene Tetracarboxylic Acid Bisimide Ligands and Metal Phosphane Triflates. *Chemistry A European Journal* **2001**, *7*, 894-902. https://doi.org/https://doi.org/10.1002/1521-3765(20010216)7:4< 894::AID-CHEM894>3.0.CO;2-N
- (64) Wu, Y.; Young, R. M.; Frasconi, M.; Schneebeli, S. T.; Spenst, P.; Gardner, D. M.; Brown, K. E.; Würthner, F.; Stoddart, J. F.; Wasielewski, M. R., Ultrafast Photoinduced Symmetry-Breaking Charge Separation and Electron Sharing in Perylenediimide Molecular Triangles. *Journal of the American Chemical Society* **2015**, *137*, 13236-13239. https://doi.org/10.1021/jacs.5b08386
- (65) Schlesinger, I.; Powers-Riggs, N. E.; Logsdon, J. L.; Qi, Y.; Miller, S. A.; Tempelaar, R.; Young, R. M.; Wasielewski, M. R., Charge-transfer biexciton annihilation in a donor–acceptor co-crystal yields high-energy long-lived charge carriers. *Chemical Science* **2020**, *11*, 9532-9541. https://doi.org/10.1039/D0SC03301D
- (66) Fink, R. F.; Seibt, J.; Engel, V.; Renz, M.; Kaupp, M.; Lochbrunner, S.; Zhao, H.-M.; Pfister, J.; Würthner, F.; Engels, B., Exciton Trapping in π-Conjugated Materials: A Quantum-Chemistry-Based Protocol Applied to Perylene Bisimide Dye Aggregates. *Journal of the American Chemical Society* **2008**, *130*, 12858-12859. https://doi.org/10.1021/ja804331b
- (67) Kaake, L. G.; Moses, D.; Heeger, A. J., Coherence and Uncertainty in Nanostructured Organic Photovoltaics. *The Journal of Physical Chemistry Letters* **2013**, *4*, 2264-2268. https://doi.org/10.1021/jz4010569
- (68) Sung, J.; Kim, P.; Fimmel, B.; Würthner, F.; Kim, D., Direct observation of ultrafast coherent exciton dynamics in helical π -stacks of self-assembled perylene bisimides. *Nature Communications* **2015**, *6*, 8646. https://doi.org/10.1038/ncomms9646
- (69) Bakalis, L. D.; Knoester, J., Pump-Probe Spectroscopy and the Exciton Delocalization Length in Molecular Aggregates. *The Journal of Physical Chemistry* **1999**, *103*, 6620-6628.
- (70) Kennehan, E. R.; Grieco, C.; Brigeman, A. N.; Doucette, G. S.; Rimshaw, A.; Bisgaier, K.; Giebink, N. C.; Asbury, J. B., Using molecular vibrations to probe exciton delocalization in films of perylene diimides with ultrafast mid-IR spectroscopy. *Phys. Chem. Chem. Phys.* **2017**, *19*, 24829-24839. https://doi.org/10.1039/C7CP04819J
- (71) Nakano, K.; Chen, Y.; Xiao, B.; Han, W.; Huang, J.; Yoshida, H.; Zhou, E.; Tajima, K., Anatomy of the energetic driving force for charge generation in organic solar cells. *Nature Communications* **2019**, *10*, 2520. https://doi.org/10.1038/s41467-019-10434-3
- (72) Liu, H.; Yin, G.; Li, Q.; Liu, G.; Pu, S.; Zhang, H., Visible-light-triggered generation of persistent radical anions from perylenediimides: A substituent effect and potential application in photocatalytic reduction of Ag+. *Dyes and Pigments* **2019**, *165*, 319-326. https://doi.org/https://doi.org/10.1016/j.dyepig.2019.02.033

- (73) Jakubka, F.; Grimm, S. B.; Zakharko, Y.; Gannott, F.; Zaumseil, J., Trion Electroluminescence from Semiconducting Carbon Nanotubes. *ACS Nano* **2014**, *8*, 8477-8486. https://doi.org/10.1021/nn503046y
- (74) Zubiria-Ulacia, M.; Matxain, J. M.; Casanova, D., The role of CT excitations in PDI aggregates. *Phys. Chem. Chem. Phys.* **2020**, *22*, 15908-15918. https://doi.org/10.1039/D0CP02344B

TOC Graphic

